

Full Length Article

The effects of copper addition on phase composition in $(\text{CrFeCo})_{1-y}\text{N}_y$ multicomponent thin films

Smita G. Rao*, Rui Shu, Robert Boyd, Arnaud le Febvrier, Per Eklund

Department of Physics, Chemistry, and Biology (IFM), Linköping University, Linköping 58183, Sweden

ARTICLE INFO

ABSTRACT

Keywords:
 Multicomponent
 Coating
 Magnetron sputtering
 High entropy alloy

The Cantor alloy CrFeCoMnNi is generally fcc structured, but moderate changes in the composition can have a large influence on the phase formation. The aim of this study was to understand the changes brought on in low-nitrogen-containing $(\text{CrFeCo})_{1-y}\text{N}_y$ thin films with $y = 0.19$ on the addition of copper, an interesting metal in terms of atomic size and nitride formation enthalpy. $(\text{CrFeCoCu}_x)_{1-y}\text{N}_y$ films were grown by reactive magnetron sputtering. The amount of copper in the films was increased from $x = 0$ to $x = 0.15$ to study competitive phase formation. Without Cu, two-phase fcc + bcc films were obtained. The addition of Cu was found to stabilize the bcc structure despite the fact that Cu as a pure metal is fcc. Nanoindentation tests showed slight increase in hardness with initial Cu addition from 11 GPa to 13.7 ± 0.2 GPa. The occurrence of pile up as opposed to cracking is an indication of the film's ductility.

1. Introduction

Multicomponent alloys, a concept which includes but is not limited to high entropy alloys (HEA), have been gaining interest due to their solid solution structure as well as the interesting properties they exhibit [1,2]. The Cantor alloy, an equimolar mixture of Fe-Cr-Mn-Ni-Co exhibiting an fcc crystal structure was one of the first multicomponent systems to be studied and now serves as a model system. The opportunity with these materials lies in tailoring the crystal structure to better the material properties.

Addition of alloying elements is one way to promote phase transformations in materials while maintaining the growth parameters. An important aspect when alloying is the atomic radii differences (δ), calculated from

$$\delta = 100 \sqrt{\sum_{i=1}^n c_i \left(1 - \frac{r_i}{r}\right)^2} \quad (1)$$

where, c_i and r_i are the atomic percentage and atomic radius of the i^{th} element, respectively and r the average atomic radius [3]. Multicomponent systems which have smaller atomic radii difference between constituent elements, such as the Cantor alloy, tend to be fcc structured while systems with larger δ are usually bcc, due to the lower packing factor of a bcc (68%) in comparison to an fcc structure (74%). The less

dense structure of a bcc, allows the larger atoms to occupy the lattice positions without causing distortions [4]. Cantor *et al.* discussed the effects of Nb, Ge, Cu, Ti and V in equimolar FeCrMnNiCo [5]. The base alloys were able to dissolve significant amounts of Nb, Ti and V resulting in fcc structured materials with an increased lattice parameter. Cu and Ge, having filled d-orbitals, were less soluble and moved to the interdendritic regions. High Cu content in the system can lead to cluster formation and phase separation due to a higher formation enthalpy with other elements in the bulk [6,7]. In the $\text{Al}_x\text{CoCrFeNi}$ alloy system, addition of Al is known to transform the crystal structure from fcc to as a consequence of the lattice distortion effect [8,9]. Adding elements such as Al and Ti to the Cantor alloy increases δ , while elements with smaller atomic radii such as Cu do not affect δ as much. Yet, they do influence the material properties.

The aim of this study was to develop a structurally stable Cantor-based thin film that could be considered as a protective coating in industry applications. Many of the materials that we use for building machines undergo stamping or deforming processes. This implies that the film/coating needs to be ductile enough to withstand the stamping process without cracking. Additions of Cu in small quantities could help to increase the ductility of the films while maintaining the crystal structure.

Obtaining single phase solid solutions is much easier in bulk alloys in comparison to thin films. The only route to stabilizing a metastable

* Corresponding author.

E-mail address: smita.gangaprasad.rao@liu.se (S.G. Rao).

phase is through quenching the bulk alloy. In thinfilm deposition, however, it is much easier to stabilize metastable phase along with additional new phases. This is due the sensitivity of the process to several factors such as the substrate, its temperature, ion flux and energy. Introducing a reactive gas, such as nitrogen or oxygen, further complicates this process. Depending on the ability of the cations to interact with the anions, various structures may be formed. For example, when considering the group 4 and 5 transition metal elements, nitrogen would occupy interstitial positions thus maintaining the NaCl structure [10,11]. However, the group 6–10 transition metals are weak nitride formers and more complex crystal phases such as intermetallic sigma phases and or combination of phases can be expected [12].

In a previous study, we studied the effects of nitrogen (~ 15 at. % to ~ 30 at. %) on the crystal structure of a simplified Cantor variant (CrFeCo) thin film where, as the amount of nitrogen increased the structure changed from fcc to bcc [13]. The stabilization of the bcc in the nitrogen containing films could be a consequence of lattice distortions, changing electronic concentrations and/or, the sputter deposition process which could result in the stabilization of phases that are in non-equilibrium conditions. The addition of an element such as Cu which does not necessarily form bonds with any of the group 6–10 metals or nitrogen due to its filled d-orbital should influence the phase formation and lattice distortion. In the present study, we aim to understand the effect of Cu addition on phase formation in low-nitrogen-content (CrFeCo)_{1-y}N_y ($y = 0.19$) thin films grown by magnetron sputtering.

2. Experimental details

A lab-scale ultrahigh vacuum magnetron sputtering system evacuated to a base pressure $< 9 \times 10^{-7}$ Pa was used to deposit CrFeCo-based nitride films. Details of the chamber can be found in reference [14]. Coatings were co-sputtered onto 2-inch diameter Si(100) substrates using four individual targets in a Ar:N₂ atmosphere with a fixed pressure of 0.4 Pa (3 mTorr) (Ar:N₂ flow ratio 54 sccm:11 sccm). The DC discharge of each magnetron (2-inch diameter target of Cr, Fe and Co) was adjusted to obtain a quasi-equiatomic composition when the Cu target power was set at 2 W. The DC power for Cr, Fe, and Co was then fixed at this value for all other depositions where the Cu target power was changed (0, 2, 4.5, 7, and 15 W) (Power density of Cr, Fe and Co ~ 4.933 W/cm², Cu-0 to 0.74 W/cm²). Prior to deposition, the substrates were cleaned by immersion in acetone and then iso-propanol for 10 min in an ultrasonic bath and blow-dried with nitrogen gas. Depositions were carried out for 30 min at a substrate temperature of 300 °C and bias -50 V.

X-ray diffraction (XRD) was carried out using a PANalytical X'Pert PRO diffractometer. All scans were performed using Cu-K α radiation ($\lambda = 1.5406$ Å) operated at a voltage of 45 kV and a current of 40 mA in a Bragg-Brentano configuration. Residual stress measurements were carried out in a PANalytical Empyrean X-ray diffractometer. The stresses were calculated from the curvature of the substrate by measuring the shift in the peak of a certain symmetrical reflection (Si 004 at 69.3°) while the angle (ω) between the incident beam and sample is changed. The Stoney equation was used to relate the curvature of the Si(100) substrate to the average stress in the film [15].

The surface and cross-section morphology of the films were characterized using a Scanning Electron Microscope (SEM LEO 1550 Gemini, Zeiss) operated at an acceleration voltage of 8 kV and using in-lens detector. The chemical composition of the films was obtained from time-of-flight elastic recoil detection analysis (ToF-ERDA). ToF-ERDA measurements were carried out at a 45° angle between the 36 MeV $^{127}\text{I}^{9+}$ primary beam incident at 67.5° and a gas ionization chamber detector in a 5 MV NEC-5SDH-2 Pelletron Tandem accelerator at Uppsala University, Sweden. The software package Potku 2.0 was used to obtain the elemental depth profiles from ToF-ERDA time and energy coincidence spectra [16].

Three samples were selected for (Scanning) Transmission Electron

Microscopy [(S)TEM] measurement. Cross-sectional TEM specimens were prepared by manual polishing down to a thickness of approximately 60 μm , followed by Ar + ion milling at 5 keV, with a 5° incidence angle, on both sides while rotating the sample in a Gatan precision ion polishing system. All analyses were performed using a FEI Tecnai G2 TF 20 UT instrument operated at 200 kV. STEM images were collected with the annular detector spanning the range 80 to 260 mrad. Elemental mapping was carried out by Energy dispersive Spectroscopy (EDS)

Nanoindentation and scratch testing was performed in a Hysitron Triboindenter 950 equipped with a 2D transducer. Indents were made on the film surface using a Berkovich tip (100 nm radius) while keeping the indentation depth below one tenth of the thickness of the coating. The hardness (H) and reduced elastic modulus (E_r) of the films were calculated according to the Oliver-Pharr method [17]. Prior to measurements, the instrument was calibrated along the indentation axis using a standard fused silica reference sample. A set of 20 indents was carried out by setting a constant load of 1.5 mN with a hold time of 5 s and delay of 30 s between each event.

The electrical resistivity of the samples was determined from the sheet resistance of the films, as measured using a four-point probe (Jandel RM3000 station). The obtained sheet resistance values were multiplied with the corresponding film thickness measured by SEM. The relevant correction factor for 50-mm-diameter substrates was used.

3. Results

3.1. Bias selection

The aim of the present study was to understand the effects of Cu on the structure of the multicomponent films. Towards this end, it was important to determine to what degree films deposited at different conditions show competition of formation between the phases. As a preliminary study, (Cr_{0.20}Fe_{0.26}Co_{0.35})N_{0.19} thin films were deposited on Si substrates with different substrate bias. This composition was chosen from our previous study [13] on the effect of nitrogen content on the properties of (CrFeCo)_{1-y}N_y thin films. Fig. 1 shows the 0–20 X-ray diffractograms and corresponding SEM images of the surface of (Cr_{0.20}Fe_{0.26}Co_{0.35})N_{0.19} samples deposited in a floating potential (I), with a bias voltage of -20 V (II), and -50 V (III). All films show a mix of fcc + bcc structures. A complete study on the competition of phases upon the addition of nitrogen can be found in our previous work [13]. The peaks at approximately 45° and 48° are identified as a bcc (110) and fcc₁ (200) structure reflections, respectively. The *d*-spacing of the

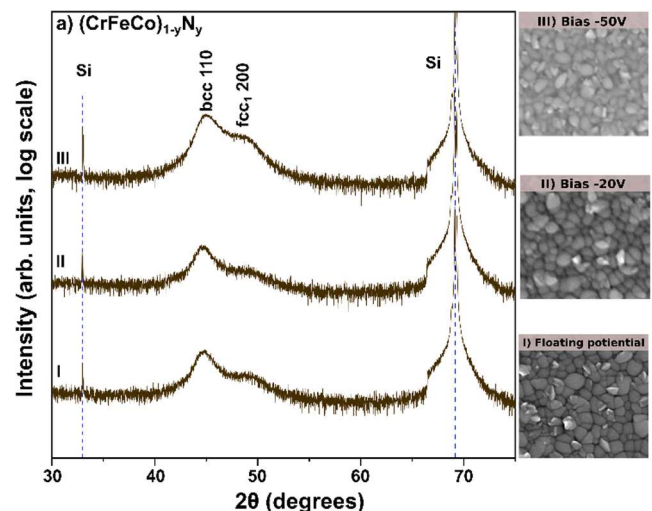


Fig. 1. X-ray diffractogram depicting the effect of substrate bias on (CrFeCo)_{1-y}N_y thin film. Inset SEM micrographs of the surface of corresponding films. Enlarged images are available in the supplementary information.

bcc 110 and fcc₁ 200 were calculated and are represented graphically in Fig. 2a and 2b respectively.

As mentioned earlier the aim of the study with addition of copper into the Cr-Fe-Co nitrogen containing system was to study the stabilization of, and competition between, phases. Since these results show that a bias voltage of -50 V induces higher crystallinity, higher preferred orientation, and lower stress along with the possibility to observe changes easily, this was used a starting point of the introduction of copper.

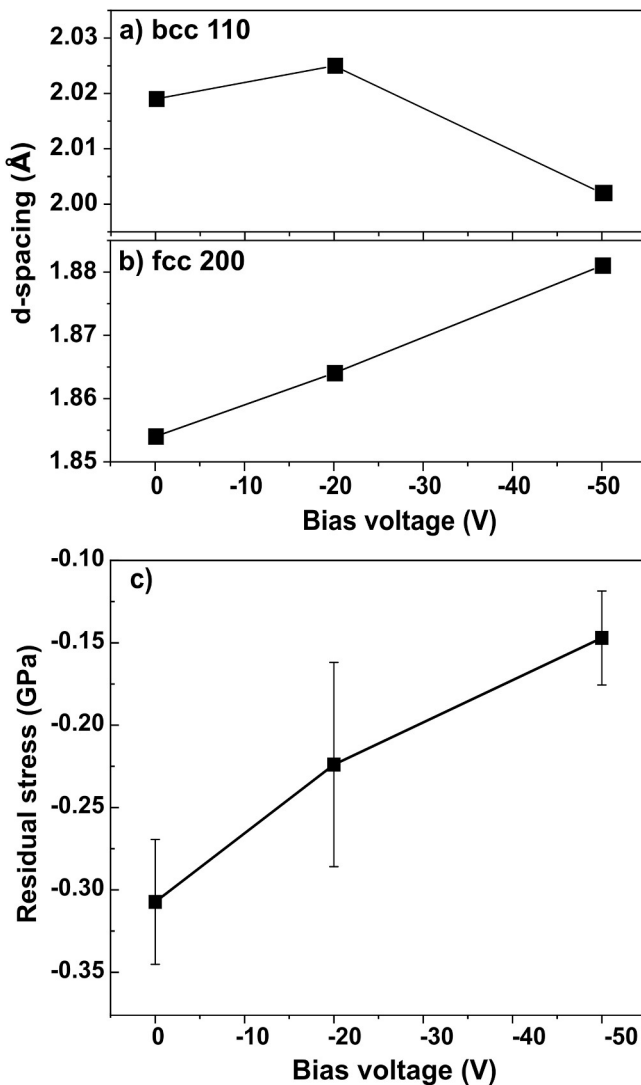


Fig. 2. Calculated d-spacing of bcc 110 peak (2a) and fcc 200 peak (2b) with increasing applied bias. (2c) Average stress of films obtained from wafer curvature measurements.

3.2. Composition

The quantification of individual metal ratios as well as estimation of nitrogen content was carried out by ToF-ERDA. Table 1 shows the changes in atomic percentages of all elements in the films as the Cu target power increased. The increase in power of the Cu target from 0 to 15 W resulted in a change in the Cu content from 0 at. % to 15 at. % in the film. For short, the samples are denoted as Cu₀ to Cu_{0.15} following the Cu content x in (CrFeCoCu_x)_{1-y}N_y. The measured variations in composition of Cr and Fe are within experimental error. The Co content, however, decreases from 35 at. % to 24 at. % as Cu is added into film. The nitrogen content was found to remain constant in all films.

3.3. Crystal structure of copper-containing films (XRD)

Fig. 3 shows the X-ray diffractograms obtained from (CrFeCoCu_x)_{1-y}N_y films with increasing Cu content. Similar to Fig. 1, substrate peaks are observed at 2θ values of 32.9° and 69.3°. The system without Cu displays a mixed fcc + bcc structure with the fcc₁ 200 peak at 49.0° and the bcc 110 peak at 44.6°. This mixed structure is also seen in Cu_{0.03}. With further addition of Cu, the 200 peak of the fcc₁ (NaCl B1-type) structure is suppressed while the bcc 110 peaks are stronger in intensity and shifted towards smaller angles caused by an increase in the cell parameter (see Table 2). The bcc structure dominates for films with x = 0.08 and 0.15 (Cu_{0.08} and Cu_{0.15}). These films were identified to be preferentially oriented along the [1 1 0] direction of a bcc structure. The Cu_{0.15} film also exhibits a peak with low intensity at 37.9° which may correspond to the (1 1 1) plane of a secondary metallic fcc structure (fcc₂).

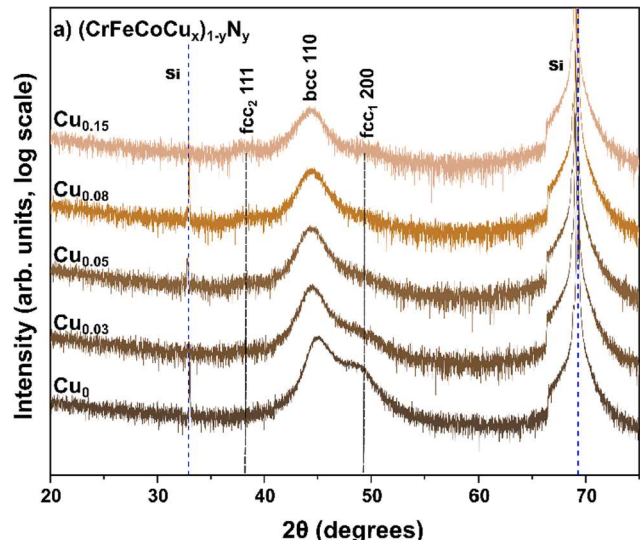


Fig. 3. X-ray diffractograms showing the effect of Cu addition into (CrFeCo)_{1-y}N_y thin films. Increasing Cu from bottom to top.

Table 1
Composition of (CrFeCoCu_x)_{1-y}N_y films estimated from ERDA.

Cu DC target power (W)	ERDA composition (± 2.00 at. %)					Thickness (nm)	General formula	Sample name
	Cr	Fe	Co	Cu	N			
0	20	26	35	0	19	520		Cu ₀
2	23	29	28	3	17	520		Cu _{0.03}
4.5	22	27	27	5	19	520	(CrFeCoCu _x) _{0.81} N _{0.19}	Cu _{0.05}
7	21	26	26	8	19	510		Cu _{0.08}
15	20	25	24	15	17	500		Cu _{0.15}

Table 2

Lattice parameters determined from the bcc 110 peak.

Sample ID	bcc a_{hkl} \pm 0.01 (Å)
Cu ₀	2.87
Cu _{0.03}	2.87
Cu _{0.05}	2.88
Cu _{0.08}	2.88
Cu _{0.15}	2.95

3.4. Morphology

Fig. 4 shows the SEM images of the surface and cross-sectional morphology of $(\text{CrFeCoCu}_x)_{1-y}\text{Ny}$ thin films. The film Cu₀ shows a columnar structure. The film has large grains with an apparent lateral average size of ~ 80 nm which are tightly packed and with well-defined grain boundaries. On addition of Cu (Cu_{0.03}, Fig. 4b), a change in morphology is noticed along with a drop in the average grain size to ~ 50 nm. With further addition of Cu (Fig. 4c-4e), the surface of the films becomes visually smoother with smaller grain sizes. Along with the change in surface morphology, changes in the film cross section are also observed. As Cu is added into the multicomponent system the apparent density increases.

3.5. TEM

Fig. 5a-c show the cross-sectional TEM images obtained from the films Cu₀, Cu_{0.03}, and Cu_{0.15}, respectively, along with inset EDS maps. Selected area electron diffraction (SAED) patterns of Cu₀, Cu_{0.03} and Cu_{0.15}, as well as their corresponding HRTEM micrographs are presented in Fig. 5d-i.

The film Cu₀ shows a columnar growth structure (Fig. 5a). The SAED pattern is consistent with a mixed fcc + bcc structure (Fig. 5d). On addition of Cu, the bcc reflections become prominent and are identified as the (110), (200), and (211) reflections with a lattice parameter of 2.92 ± 0.02 Å. The change from spots to more continuous rings is an indication of the change in orientation of grains from preferential orientation to random as well as increasing polycrystallinity of the films (Fig. 5e and 5f). Cross-sectional TEM and HRTEM micrographs of Cu_{0.03} and Cu_{0.15}, show a dense film with no prominent columns or pores as observed in the SEM cross sections (Fig. 4b-e). In the case of Cu₀, no apparent inhomogeneity in the composition is observed. Cu_{0.03} also shows a homogenous distribution of elements along the film as seen in the inset in Fig. 5b. However, the Cu_{0.15} film presents the segregation of copper (inset, Fig. 5c).

3.6. Mechanical properties (nanoindentation)

Measured residual stresses are shown in Fig. 6a. The film with no Cu, Cu₀ had a compressive stress of 0.2 GPa. On addition of copper the stress increase reaching a maximum ~ 0.5 GPa for Cu_{0.05}. The stress is seen to reduce with further increase of Cu as in the case of Cu_{0.08} and Cu_{0.15}. Fig. 6b shows the hardness values as a function of the Cu content in the $(\text{CrFeCoCu}_x)_{1-y}\text{Ny}$ films. An indentation creep of approximately 5 nm was observed between Cu_{0.03} and Cu_{0.15}. Load-displacement curves can be found in the [supplementary information](#). All films have hardness values ranging between 10 and 14 GPa, as expected for Cantor alloy thin films and their variants [2,18,19]. The film with no Cu exhibits a hardness of approximately 11 ± 1 GPa. On addition of Cu, the hardness is seen to increase to 13.7 ± 0.2 GPa (Cu_{0.05}). Youngs modulus of the films is also seen to reduce on the addition of Cu from 208 ± 0.2 to 180 ± 0.5 GPa (Fig. 6c).

Fig. 7 is a SEM image of Cu_{0.05} after an indentation event. The image shows the plastic deformation that has taken place by the presence of pile up of material along the outer edges of the indent.

The resistivity of the films was measured by four-point probe. The

films Cu₀ along with the lowest hardness also displayed the highest resistivity of 28 ± 1 $\mu\Omega\text{cm}$. On addition of Cu the resistivity was seen to drop to 26 ± 1 $\mu\Omega\text{cm}$ for Cu_{0.03} and 17 ± 1 $\mu\Omega\text{cm}$ for Cu_{0.15}.

4. Discussion

4.1. Phase stabilization

In our previous study on the nitrogen containing Cr-Fe-Co system, thin films with a mixed fcc + bcc structure were observed [13]. The stabilization of the bcc in low-nitrogen-content films may appear surprising at first sight; however, it is not in itself unlikely. On addition of Cu, the first change observed is the reduction in the amount of Co in the film. The initial suppression of the fcc 200 as seen in film Cu_{0.03} could be a consequence of the decreasing Co as well as the addition of Cu. This argument, however, holds only for Cu_{0.03}. Further increase of Cu in the film (Cu_{0.05}-Cu_{0.15}) does not have as much effect on the individual metal ratios. Therefore, it is possible that the phase stabilization taking place is in fact due to the introduction of Cu. As the amount of Cu is increased from $x = 0.08$ to 0.15, a secondary phase is observed with the appearance of a peak at $\sim 37^\circ$ corresponding to the (111) plane of an fcc structure (Fig. 3) from Cu segregating in the film. A comparative study on CrCoCuFeNi bulk as well as thin films showed similar results where no segregation occurred in thin films up to 8 at.-% [20]. The limit of Cu solubility into the multicomponent matrix followed a similar trend. In the case of Cu_{0.15} the segregation may be due the inability of Cu to bond with the other elements in the thin film thus forming a secondary metallic fcc structure. The appearance of a ring with d spacing of 2.44 Å on Cu_{0.15} along with STEM images provides further evidence for the segregation and secondary fcc structure formation (inset Fig. 5c and 5f).

4.2. Morphology

The film Cu₀, exhibited a columnar growth structure, which is generally associated with low surface diffusion of the accelerated particles and leads to the formation of dome shaped structures on the film surface as seen in Fig. 4a [21]. The HRTEM image of Cu₀ (Fig. 5g) indicates a possible interface between two other fibres. As copper is introduced into the $(\text{CrFeCo})_{1-y}\text{Ny}$ matrix the apparent density of the films increases (Fig. 5e-f) [21]. It is possible that, with the addition of Cu, the energy brought to the substrate increases thus promoting surface diffusion of the ions leading to small, densely packed, and randomly oriented grains. The stress in the films also increases with the initial addition of Cu. This may validate the fact that energy brought to the substrate is higher. Studies on polycrystalline Fe thin films suggest that smaller grains lead to higher compressive stresses [22,23]. On further addition of Cu, as in the case of Cu_{0.15}, the film is almost stress free or under a small tensile stress. The change in stress from compressive to tensile with addition of Cu may be a result of grain boundary relaxation and a smaller number of defects and dislocations [24].

The question is: Would the same stabilization effect be observed if a different metal were used instead of Cu? As previously mentioned, the stabilization effect on bcc by the addition of Al or an element which has significantly larger atomic radius in comparison to the group 6–10 metals is well known. The effects of higher concentration or addition of a group 6–10 metal are not as clear but would depend on their ability to form nitrides. The magnetic properties of these elements may also influence the phase formation [25–27]. However, it is known that variants of the Cantor alloy do not always form fcc structures and phase formation is very different in comparison to multicomponent alloys and thin films of the refractory metals [28].

4.3. Mechanical properties

The mechanical properties of the films are clearly influenced by the morphology. As the amount of Cu in the films' is increased the apparent

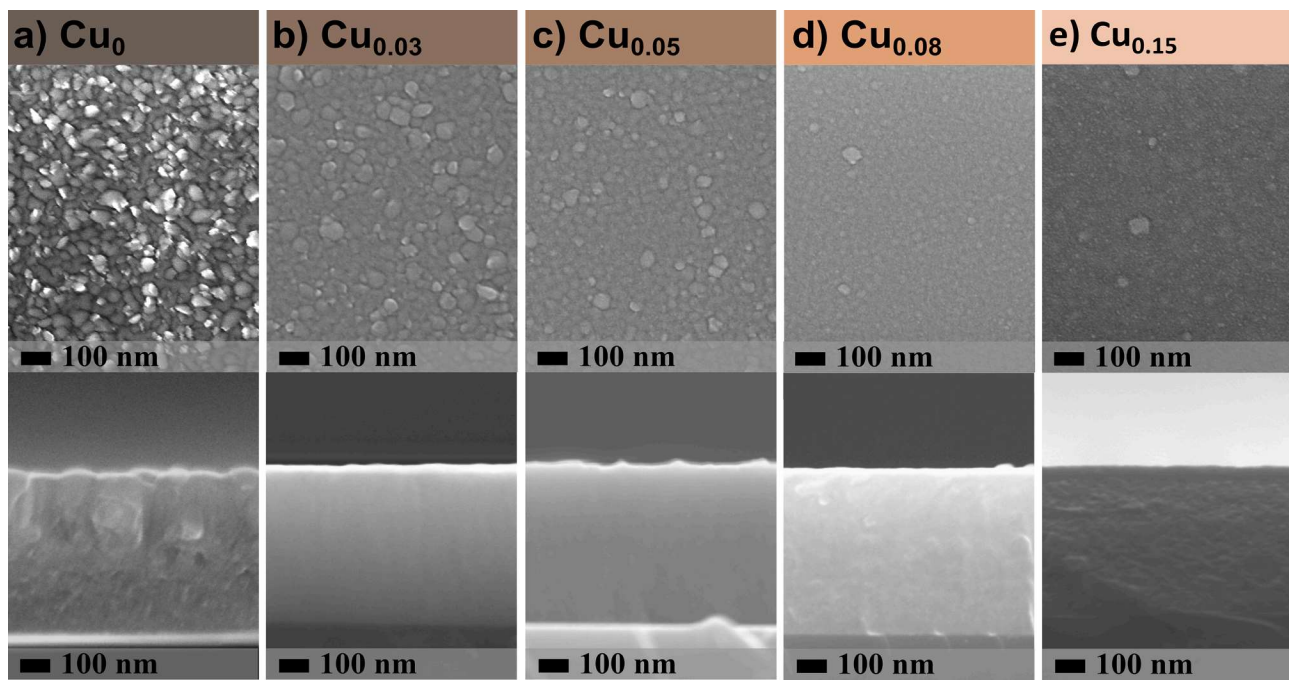


Fig. 4. Top view and corresponding cross-section SEM micrographs of $(\text{CrFeCoCu}_x)_{1-y}\text{N}_y$ films with Cu content increasing from a to e.

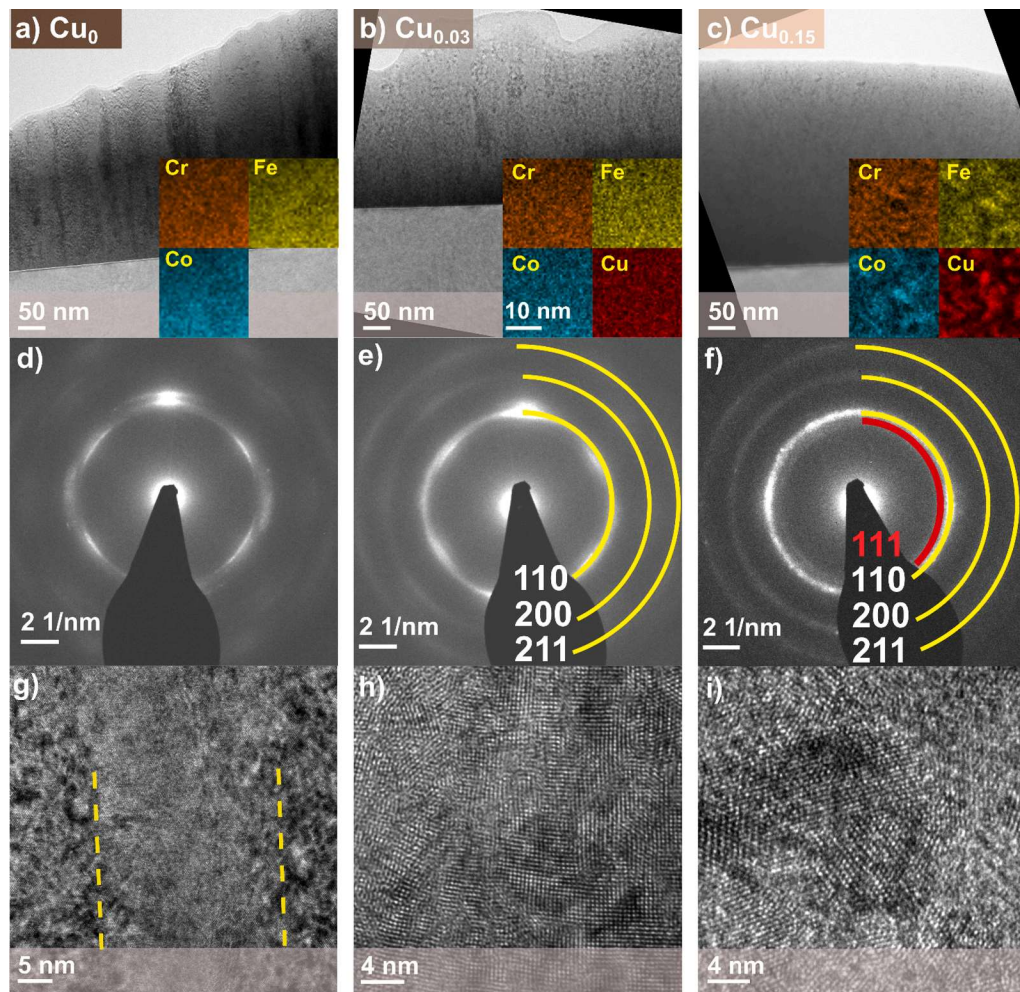


Fig. 5. TEM bright field images of films (5a, 5b, 5c) with inset EDS maps; SAED patterns (5d, 5e, 5f), corresponding HRTEM images (5 g, 5 h, 5i).

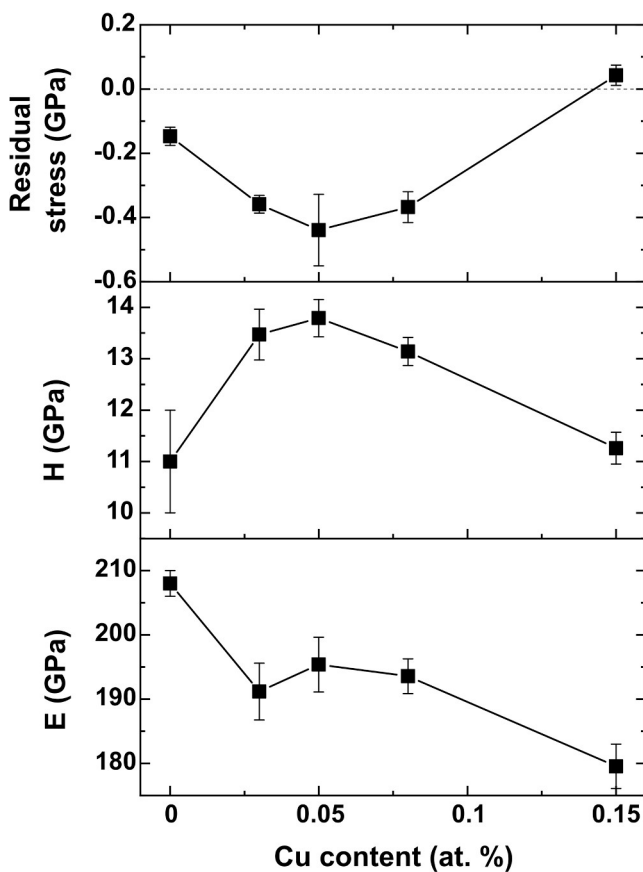


Fig. 6. a) Residual stresses in $(\text{CrFeCuCu}_x)_{1-y}\text{N}_y$ thin films calculated from wafer curvature measurements; (b,c) corresponding hardness (H) and Young's modulus (E) values.

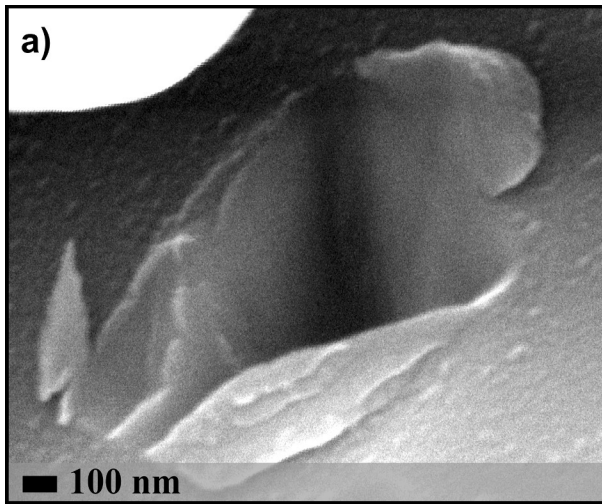


Fig. 7. Occurrence of pile up in $\text{Cu}_{0.05}$ after an indentation event.

density of the films increases while grain size reduces as seen in SEM images (Fig. 4c). The higher hardness observed in $\text{Cu}_{0.05}$ and $\text{Cu}_{0.08}$ may be a result of the decrease in the competition between phases and stabilization of the bcc over the fcc and the increasing random orientation of the grains which may inhibit the propagation of dislocations resulting in grain refinement strengthening. As the Cu content is further increased to $x = 0.15$ ($\text{Cu}_{0.15}$) the hardness is seen to fall to ~ 11 GPa this indicated the softening of the films. The segregation of Cu observed on the

STEM-EDS maps may be a reason for the drop in hardness along with the decrease in the stress. The absence of cracks as well as pile up around the edges of the indent are an indication of the ductility of the films.

5. Conclusion

$(\text{CrFeCoCu}_x)_{1-y}\text{N}_y$ films were grown on Si substrates by reactive magnetron sputtering. The copper content in the films was increased from $x = 0$ to $x = 0.15$ by controlling the target power. The changes in the thin film crystal structure and properties were studied. XRD revealed that as Cu is added into an originally fcc + bcc mixed phase film, the bcc is stabilised. SEM and TEM shows that the apparent film density increased with addition of Cu into the Cr-Fe-Co-N matrix. As the Cu_x increases content from $x = 0$ to $x = 0.15$ the energy brought to the substrate increases, promoting surface diffusion of the ions and leading to small, randomly oriented grains. The maximum hardness recorded by nanoindentation was found to be 13.7 ± 0.2 GPa for the sample $\text{Cu}_{0.05}$. The present study showed that small amounts (0–5 at. %) of Cu in the multicomponent matrix could be beneficial in stabilizing phases as well as improving mechanical properties.

CRediT authorship contribution statement

Smita G. Rao: Conceptualization, Investigation, Data curation, Formal analysis, Writing – original draft. . **Rui Shu:** Investigation, Formal analysis. **Robert Boyd:** Investigation, Formal analysis. **Arnaud le Febvrier:** Conceptualization, Investigation, Supervision, Formal analysis, Writing – review & editing. **Per Eklund:** Project administration, Conceptualization, Supervision, Writing – review & editing, Funding acquisition.

Declaration of Competing Interest

The authors declare that they have no known competing financial interests or personal relationships that could have appeared to influence the work reported in this paper.

Acknowledgements

This work is supported by the VINNOVA Competence Centre FunMat-II (grant no. 2016-05156), the Swedish Government Strategic Research Area in Materials Science on Functional Materials at Linköping University (Faculty Grant SFO-Mat-LiU No. 2009 00971). The Knut and Alice Wallenberg Foundation is acknowledged for support through the Wallenberg Academy Fellows program (P.E., grant number 2020.0196) and the Electron Microscopy Laboratory at Linköping University. Daniel Primetzhofer at Uppsala University is acknowledged for assistance with ERDA measurements at the Tandem Laboratory infrastructure, financed by the Swedish Research Council via VR-RFI contract C0514401 and by the Swedish Foundation for Strategic Research via SSF contract RIF14-0053.

Appendix A. Supplementary material

Supplementary data to this article can be found online at <https://doi.org/10.1016/j.apsusc.2021.151315>.

References

- [1] D.B. Miracle, O.N. Senkov, A critical review of high entropy alloys and related concepts, *Acta Mater.* 122 (2017) 448–511, <https://doi.org/10.1016/j.actamat.2016.08.081>.
- [2] C. Dang, J.U. Surjadi, L. Gao, Y. Lu, Mechanical properties of nanostructured CoCrFeNiMn High-Entropy Alloy (HEA) coating, *Front. Mater.* 5 (2018) 41, <https://doi.org/10.3389/fmats.2018.00041>.
- [3] Y. Zhang, Y.J. Zhou, J.P. Lin, G.L. Chen, P.K. Liaw, Solid-solution phase formation rules for multi-component alloys, *Adv. Eng. Mater.* 10 (6) (2008) 534–538, <https://doi.org/10.1002/adem.200700210>.

- [doi.org/10.1002/\(ISSN\)1527-264810.1002/adem.v10:610.1002/adem.200700240](https://doi.org/10.1002/(ISSN)1527-264810.1002/adem.v10:610.1002/adem.200700240).
- [4] S.A. Kube, S. Sohn, D. Uhl, A. Datye, A. Mehta, J. Schroers, Phase selection motifs in High Entropy Alloys revealed through combinatorial methods: Large atomic size difference favors BCC over FCC, *Acta Mater.* 166 (2019) 677–686, <https://doi.org/10.1016/j.actamat.2019.01.023>.
- [5] B. Cantor, I.T.H. Chang, P. Knight, A.J.B. Vincent, Microstructural development in equiatomic multicomponent alloys, *Mater. Sci. Eng. A.* 375–377 (2004) 213–218, <https://doi.org/10.1016/j.msea.2003.10.257>.
- [6] C.-J. Tong, Y.-L. Chen, S.-K. Chen, J.-W. Yeh, T.-T. Shun, C.-H. Tsau, S.-J. Lin, S.-Y. Chang, Microstructure characterization of AlxCrCuFeNi High-Entropy Alloy system with multiprincipal elements.
- [7] B. Gwalani, D. Choudhuri, V. Soni, Y. Ren, M. Styles, J.Y. Hwang, S.J. Nam, H. Ryu, S.H. Hong, R. Banerjee, Cu assisted stabilization and nucleation of L12 precipitates in Al0.3CuFeCrNi2 fcc-based high entropy alloy, *Acta Mater.* 129 (2017) 170–182, <https://doi.org/10.1016/j.actamat.2017.02.053>.
- [8] W.R. Wang, W.L. Wang, S.C. Wang, Y.C. Tsai, C.H. Lai, J.W. Yeh, Effects of Al addition on the microstructure and mechanical property of AlxCrFeNi high-entropy alloys, *Intermetallics.* 26 (2012) 44–51, <https://doi.org/10.1016/j.intermet.2012.03.005>.
- [9] J.-W. Yeh, Recent progress in high-entropy alloys, *Ann. Chim. Sci. Des Mater.* 31 (6) (2006) 633–648, <https://doi.org/10.3166/acsm.31.633-648>.
- [10] H.-P. Chou, Y.-S. Chang, S.-K. Chen, J.-W. Yeh, Microstructure, thermophysical and electrical properties in AlxCrCoFeNi ($0 \leq x \leq 2$) high-entropy alloys, *Mater. Sci. Eng. B Solid-State Mater. Adv. Technol.* 163 (3) (2009) 184–189, <https://doi.org/10.1016/j.msrb.2009.05.024>.
- [11] P.-K. Huang, J.-W. Yeh, Effects of substrate bias on structure and mechanical properties of (AlCrNbSiTiVN) coatings, *J. Phys. D. Appl. Phys.* 42 (11) (2009) 115401, <https://doi.org/10.1088/0022-3727/42/11/115401>.
- [12] E. Lewin, Multi-component and high-entropy nitride coatings—A promising field in need of a novel approach, *J. Appl. Phys.* 127 (16) (2020) 160901, <https://doi.org/10.1016/j.jap.2019.15144154>.
- [13] S.G. Rao, R. Shu, R. Boyd, G. Greczynski, A. le Fevrier, P. Eklund, Phase formation and structural evolution of multicomponent (CrFeCo)Ny films, *Surf. Coatings Technol.* (2021), 127059, <https://doi.org/10.1016/j.surcoat.2021.127059>.
- [14] A. le Fevrier, L. Landälv, T. Liersch, D. Sandmark, P. Sandström, P. Eklund, An upgraded ultra-high vacuum magnetron-sputtering system for high-versatility and software-controlled deposition, *Vacuum.* 187 (2021) 110137, <https://doi.org/10.1016/j.vacuum.2021.110137>.
- [15] G.C.A.M. Janssen, M.M. Abdalla, F. van Keulen, B.R. Pujada, B. van Venrooy, Celebrating the 100th anniversary of the Stoney equation for film stress: Developments from polycrystalline steel strips to single crystal silicon wafers, *Thin Solid Films.* 517 (6) (2009) 1858–1867, <https://doi.org/10.1016/j.tsf.2008.07.014>.
- [16] K. Arstila, J. Julin, M.I. Laitinen, J. Aalto, T. Konu, S. Kärkkäinen, S. Rahkonen, M. Raunio, J. Itkonen, J.P. Santanen, T. Tuovinen, T. Sajavaara, Potku - New analysis software for heavy ion elastic recoil detection analysis, *Nucl. Instruments Methods Phys. Res. Sect. B Beam Interact. with Mater. Atoms.* 331 (2014) 34–41, <https://doi.org/10.1016/j.nimb.2014.02.016>.
- [17] W.C. Oliver, G.M. Pharr, An improved technique for determining hardness and elastic modulus using load and displacement sensing indentation experiments, *J. Mater. Res.* 7 (6) (1992) 1564–1583, <https://doi.org/10.1557/JMR.1992.1564>.
- [18] Z.e. Wang, C. Wang, Y.-L. Zhao, Y.-C. Hsu, C.-L. Li, J.-J. Kai, C.-T. Liu, C.-H. Hsueh, High hardness and fatigue resistance of CoCrFeMnNi high entropy alloy films with ultrahigh-density nanotwins, *Int. J. Plast.* 131 (2020) 102726, <https://doi.org/10.1016/j.ijplas.2020.102726>.
- [19] Y.S. Kim, H.J. Park, K.S. Lim, S.H. Hong, K.B. Kim, Structural and mechanical properties of AlCoCrNi high entropy nitride films: Influence of process pressure, *Coatings.* 10 (1) (2020) 10, <https://doi.org/10.3390/coatings1001010>.
- [20] Z. An, H. Jia, Y. Wu, P.D. Rack, A.D. Patchen, Y. Liu, Y. Ren, N. Li, P.K. Liaw, Solid-solution CrCoCuFeNi high-entropy alloy thin films synthesized by sputter deposition, *Mater. Res. Lett.* 3 (4) (2015) 203–209, <https://doi.org/10.1080/21663831.2015.1048904>.
- [21] J.A. Thornton, The microstructure of sputter-deposited coatings, *J. Vac. Sci. Technol. A Vacuum, Surfaces, Film.* 4 (6) (1986) 3059–3065, <https://doi.org/10.1116/1.573628>.
- [22] R. Koch, D. Hu, A.K. Das, Compressive stress in polycrystalline Volmer-Weber films, <https://doi.org/10.1103/PhysRevLett.94.146101>.
- [23] G. Abadias, E. Chason, J. Keckes, M. Sebastiani, G.B. Thompson, E. Barthel, G. L. Doll, C.E. Murray, C.H. Stoessel, L. Martinu, Review Article: Stress in thin films and coatings: Current status, challenges, and prospects, *J. Vac. Sci. Technol. A Vacuum, Surfaces, Film.* 36 (2) (2018) 020801, <https://doi.org/10.1116/1.5011790>.
- [24] R. Abermann, Measurements of the intrinsic stress in thin metal films, *Vacuum.* 41 (4–6) (1990) 1279–1282, [https://doi.org/10.1016/0042-207X\(90\)93933-A](https://doi.org/10.1016/0042-207X(90)93933-A).
- [25] V. Chaudhary, B. Gwalani, V. Soni, R.V. Ramanujan, R. Banerjee, Influence of Cr substitution and temperature on hierarchical phase decomposition in the AlCoFeNi high entropy alloy, *Sci. Rep.* 8 (2018) 15578, <https://doi.org/10.1038/s41598-018-33922-w>.
- [26] V. Chaudhary, R.V. Ramanujan, Magnetocaloric properties of Fe-Ni-Cr nanoparticles for active cooling, *Sci. Rep.* 6 (2016) 1–9, <https://doi.org/10.1038/srep35156>.
- [27] T. Borkar, V. Chaudhary, B. Gwalani, D. Choudhuri, C.V. Mikler, V. Soni, T. Alam, R. V. Ramanujan, R. Banerjee, A combinatorial approach for assessing the magnetic properties of high entropy alloys: Role of Cr in AlCo x Cr 1-x FeNi, *Adv. Eng. Mater.* 19 (8) (2017) 1700048, <https://doi.org/10.1002/adem.201700048>.
- [28] M.K. Kini, S. Lee, A. Savan, B. Breitbach, Y. Addab, W. Lu, M. Ghidelli, A. Ludwig, N. Bozzolo, C. Scheu, D. Chatain, G. Dehm, Nanocrystalline equiatomic CoCrFeNi alloy thin films: Are they single phase fcc? *Surf. Coatings Technol.* 410 (2021) 126945, <https://doi.org/10.1016/j.surcoat.2021.126945>.